Available online at www.sciencedirect.com
ScienceDirect
Journal of Sound and Vibration 306 (2007) 601–617
JOURNAL OF SOUND AND VIBRATION
www.elsevier.com/locate/jsvi

# Dynamic simulation of a flexible rotor during drop on retainer bearings

Antti Kärkkäinen[a,*], Jussi Sopanen[b], Aki Mikkola[a]

[a]Department of Mechanical Engineering, Lappeenranta University of Technology, P.O. Box 20, FI-53851 Lappeenranta, Finland
[b]Mechanical Engineering and Production Technology, South Carelia Polytechnic, Pohjolankatu 23, FI-53101 Lappeenranta, Finland

Received 23 October 2006; received in revised form 1 April 2007; accepted 30 May 2007
Available online 13 July 2007

**Abstract**

Active magnetic bearings (AMBs) present a technology which has many advantages compared to traditional bearing concepts. However, they require retainer bearings in order to prevent damages in the event of a system failure. In the drop-down when the rotor falls from the magnetic field on the retainer bearings, the design of the retainer bearings has a significant influence on the dynamic behavior of the rotor. In this study, the dynamics of an active magnetic bearing supported rotor during the drop on retainer bearings is studied employing a detailed simulation model. The retainer bearings are modeled using an accurate ball bearing model which takes into account damping and stiffness properties, oil film, inertia of rolling elements and friction between races and rolling elements. The model of a flexible rotor system accounts for unbalances as well as stiffness and damping properties of the support. In this study, the flexibility of the rotor is described using the finite element approach with the component mode synthesis. This study sheds light on the effects of a number of modes used in the component mode synthesis on the accuracy of simulated responses during the drop-down. In addition, the effect of different friction models on the behavior of the rotor is examined.


## 1. Introduction

The area of active magnetic bearings (AMBs) has been recently developed intensively because the non-contact support provided by AMBs has several advantages compared to conventional bearings. The most important advantages are non-existent friction and, consequently, little energy loss, the lack of need for lubrication, and quiet operation. An AMB provides adjustable stiffness and damping, which makes accurate rotor positioning possible. In addition, AMBs offer active control over the rotor that they support. Adjustable stiffness and damping is beneficial particularly from the mechanical point of view. AMBs allow for the controlling of the natural frequencies and damping properties of the rotor system during operation. As a result, the vibration of the rotor can be controlled, and the rotor supported by AMBs can be operated at supercritical speeds. Due to the active feedback control of AMBs, unbalance compensation during rotor operation is also possible. In the unbalance compensation, the rotor does not rotate around its geometrical

*Corresponding author. Tel.: +358 5 621 2468; fax: +358 5 621 2499.
*E-mail address:* antti.karkkainen@lut.fi (A. Kärkkäinen).

0022-460X/$ - see front matter © 2007 Elsevier Ltd. All rights reserved.
doi:10.1016/j.jsv.2007.05.047

center; instead, it rotates around its main inertia principal axis. It is important to note that the rotation around the main inertia principal axis is not possible when using rolling element bearings. The most important mechanical parts in AMBs are widely known, as well as the operation principle of bearings [1]. Compressors, generators, machine tools, and electric motors are the most general applications of AMBs. Due to improved materials, strategies of control, and electric components, the performance and reliability of AMBs are improving. However, additional bearings, the retainer bearings, still have a vital role in AMB applications. The most crucial moment when the retainer bearings are needed is when the rotor drops from the AMBs on retainer bearings caused by component or power failure [1–3]. Without appropriate knowledge of retainer bearings, there is a chance that an AMB supported rotor system will be fatal in a drop-down situation.

Retainer bearings can be categorized into three types. Bushing type retainer bearings are simple, and consequently inexpensive and easy to repair when necessary. However, the friction properties of bushing type retainer bearings can change during deceleration of a rotor due to the wearing of a sleeve. Wearing typically increases the friction force, resulting in changes in the dynamic behavior of the rotor. Due to the high friction caused by wearing, bushing type retainer bearings are often unable to dissipate the energy of the rotor without the rotor becoming unstable. For this reason, bushing type retainer bearings are normally replaced after a low number of high speed drop-downs. Retainer bearings based on a rolling element bearing are mechanically more complicated, and therefore also more sensitive to impacts. The rolling element bearing stabilizes the motion of the rotor after drop-down because the inner race rapidly achieves the angular velocity of the rotor. This may prevent the whirling motion of the rotor. This is due to the fact that in a rolling condition, the relative velocity between the rotor and the inner race of the bearing is virtually zero [4]. The third type of retainer bearing is a combination of the two previously mentioned. However, this type of bearing suffers from some drawbacks, such as a large moment of inertia of rotating parts. This can lead to slower acceleration to the speed of the rotor when compared to traditional rolling element type retainer bearings. Investigations on hybrid backup bearings [5] and zero clearance backup bearings [6] have also been carried out in order to improve backup bearing technology. In addition, an active auxiliary bearing that is attached to the foundation through unidirectional electromagnetic actuators is presented in the literature [7].

The most frequently examined characteristics of retainer bearings are stiffness, damping and friction coefficients between the rotor and bearing. The effects of those coefficients are widely known, as reviewed by Ecker [8], Zeng [9], Ishii and Kirk [2]. Cole et al. [10,11] examined the dynamic behavior of the rolling element bearing after rotor impact. They pointed out that the inner race of the bearing should be allowed to accelerate as rapidly as possible in order to minimize the energy dissipation in the bearing and consequently minimize the likelihood of friction-induced whirling motion of the rotor. Raju et al. [12] performed a similar examination to Cole et al. [10] using solid brass backup bearings. However, both of the results are useful in practical design only when designing retainer bearings similar to those they examined. The dynamic behavior of bushing and rolling bearing type retainer bearings differs considerably, as the investigations carried out by Fumagalli [4] and Swanson et al. [13] have proved. The emergency drop-down of the rotor is usually caused by a component, power or control system failure. It is noteworthy that researchers have different estimations regarding the effect of the collapsing magnetic force on the drop-down behavior of the rotor. Zeng [14] mentioned in his examination that the effect of the collapsing magnetic force of the failed AMB might be ignored in the analysis. On the other hand, Orth et al. [3] compared the results of Fumagalli [4] with their own examinations and suggested that the reason for the discrepancy between the examinations is the collapsing magnetic field of the AMBs that is still producing a decreasing magnetic force.

Common to all above-mentioned examinations is that they are based on the finite element model [15], conventional rotor dynamics or experimental studies. In most of the cases, the rotor is described by using Jeffcott's rotor model and simple bearing models. The objective of this study is to build a detailed simulation model of the AMB system in order to describe the rotor drop-down on the retainer bearings. The introduced simulation model couples a finite element model, modal reduction and a detailed bearing model. The retainer bearings are described using a ball bearing model which includes damping and stiffness properties, oil film, inertia of rolling elements and friction between the races and rolling elements. The model of the AMB system includes unbalances of the flexible rotor, which is modeled by using the finite element approach. The stiffness and damping properties of the support are included in the model.

In this study, the focus is on the dynamics of the mechanical components of the AMB system, whereas electrical components and electromechanical forces are not considered. This study sheds light on the effects of a number of modes used in the component mode synthesis on the accuracy of simulated responses during the drop-down. The unstabilizing effect of the natural frequency of the rotor during rundown is also explained in this study. In addition, the effect of various friction models and radial clearance of the retainer bearing on the behavior of the rotor system is described in this study.

## 2. Models of rotor and backup bearings

Models of the rotor, bearing and contact are presented in this section. The model of the rotor is accomplished by using the finite element approach. In this study, the ball bearing model previously introduced by Sopanen and Mikkola [16,17] is employed.

### 2.1. Models of the flexible rotor

The rotor under investigation is modeled using beam finite elements. The beam elements are based on the Timoshenko beam theory, which accounts for the shear deformation. In this study, the analysis of the rotor is focused on the lateral vibration, and for this reason, axial and torsion degrees of freedom are neglected in the beam element. The cross-section of the element is assumed to remain undeformable, and thus the configuration of the element can be parameterized by employing the centerline of the element. The detailed implementation of a flexible rotor by using finite elements is explained in Refs. [18–20]. In the finite element approach, equations of motion for a rotor bearing system with a variable rotation speed can be written as follows:

$$\mathbf{M}\ddot{\mathbf{q}} + (\mathbf{C} + \Omega\mathbf{G})\dot{\mathbf{q}} + (\mathbf{K} + \dot{\Omega}\mathbf{G})\mathbf{q} = \Omega^2\mathbf{Q}_1 + \dot{\Omega}\mathbf{Q}_2 + \mathbf{F}, \tag{1}$$

where $\mathbf{M}$ is the mass matrix, $\mathbf{C}$ is the damping matrix, which in this study is defined using experimental modal analysis, $\mathbf{G}$ is the gyroscopic matrix and $\mathbf{K}$ is the stiffness matrix. Vector $\mathbf{q}$ is the vector of system nodal coordinates, $\mathbf{F}$ the vector of externally applied forces and $\Omega$ the angular velocity of the rotor. Force vectors $\mathbf{Q}_1$ and $\mathbf{Q}_2$ describe the mass unbalance of the rotor. For a system with a constant angular velocity, Eq. (1) can be simplified as follows:

$$\mathbf{M}\ddot{\mathbf{q}} + (\mathbf{C} + \Omega\mathbf{G})\dot{\mathbf{q}} + \mathbf{K}\mathbf{q} = \Omega^2\mathbf{Q}_1 + \mathbf{F}. \tag{2}$$

Both Eqs. (1) and (2) can be solved by using a standard time integration scheme. However, a numerical solution may be time consuming since equations may include high frequencies and the dimensions of the matrices may be large. The number of the degrees of freedom of the system can be reduced using the component mode synthesis [21,22]. In this approach, modal coordinates, instead of nodal coordinates, are used in the equation of motion. In the component mode synthesis, high frequency modes can be neglected without a significant loss of accuracy. This is realistic because, in practice, only the lowest frequency modes contribute significantly to the response of the system. This approach will also lead to diagonal matrices in the description of mass, stiffness and damping matrices. By using modal coordinates, Eq. (1) can be re-written as follows:

$$\mathbf{\Phi}^{\mathrm{T}}\mathbf{M}\mathbf{\Phi}\ddot{\mathbf{p}} + (\mathbf{\Phi}^{\mathrm{T}}\mathbf{C}\mathbf{\Phi} + \Omega\mathbf{\Phi}^{\mathrm{T}}\mathbf{G}\mathbf{\Phi})\dot{\mathbf{p}} + (\mathbf{\Phi}^{\mathrm{T}}\mathbf{K}\mathbf{\Phi} + \dot{\Omega}\mathbf{\Phi}^{\mathrm{T}}\mathbf{G}\mathbf{\Phi})\mathbf{p} = \mathbf{\Phi}^{\mathrm{T}}\mathbf{F}_{\mathrm{tot}}, \tag{3}$$

where $\mathbf{\Phi}$ is the mode matrix of the rotor, $\mathbf{p}$ is a vector of modal coordinates and $\mathbf{F}_{\mathrm{tot}}$ is a vector of the sum of applied forces. The vector of modal coordinates can be solved using a standard time integration scheme. A drawback associated with the component mode synthesis is the matrix multiplication that is needed when physical forces are transformed into modal forces and when modal coordinates are transformed into physical coordinates. However, in AMB applications only a few bearing forces are used and only a few sensor displacements are needed during the solution of the equations of motion. For this reason, the transformations can be simplified and the multiplication of full matrices may not be necessary.

## 2.2. Model of ball bearing

### 2.2.1. Bearing force calculation

In this study, the bearing model introduced by Sopanen and Mikkola [16] is used in the dynamic analysis of the drop-down of the rotor. A ball bearing consists of a number of moving parts. When describing the responses of each part, a simulation model consists of a large number of degrees of freedom, and for this reason it may be computationally excessively expensive. In this study, the bearing model ignores the centrifugal forces of the balls and assumes that the cage of the bearing is ideal. In practice, this means that the cage holds the balls in their predefined positions precisely. In the bearing model, it is also assumed that no slipping or sliding occurs between the components of the bearing. This assumption may not be valid in the acceleration of the retainer bearings. The assumption is, however, frequently used in studies of retainer bearings [4,23]. Cole et al. [10] demonstrated the significance of sliding by using a full complement bearing model. In the research, it is noted that rapid acceleration of the inner race may result in a zone of sliding balls on the opposite side of the bearing to the impact, where ball loading is small. Helfert et al. [24] have studied the dynamics of a cageless bearing and showed that the individual ball of the bearing achieved the full rotation speed almost at the same time as the inner ring of the bearing. After this instant, the velocity of the ball oscillates before it stabilizes to the velocity of the rotor. Based on the two above-mentioned studies, the significance of sliding between the balls and races is important when the dynamics of an individual ball or the bearing itself is examined. However, sliding between the balls and races can be disregarded when considering the dynamics of the entire rotor system. It is also noteworthy that in the case of the bearing with a cage, sliding of the ball in the zone of small ball loading is less significant compared to the case of the cageless bearing.

The original bearing model proposed by Sopanen and Mikkola [16] included six degrees of freedom. In this study, the bearing model is simplified in such a way that it takes only radial displacements and the rotation around the bearing axis into account. The ball bearing model includes descriptions of nonlinear Hertzian contact deformation and elastohydrodynamic fluid film thickness. The geometry, such as the outer and inner diameter of the bearing and clearances, and material properties are given as an input to the model. In this section, the description of resultant bearing forces acting upon the rotor in the radial directions is briefly reviewed. A detailed description of the bearing model can be found from Ref. [16]. The contact force acting on the ball $i$ can be obtained as follows [25]:

$$F_i = K_c^{\mathrm{tot}}(\delta_i^{\mathrm{tot}})^{3/2}, \tag{4}$$

where $K_c{}^{\mathrm{tot}}$ is the total stiffness coefficient of the bearing and $\delta_i{}^{\mathrm{tot}}$ is the total elastic deformation. The total stiffness coefficient accounts for both the inner and outer race contacts and can thus be expressed as follows:

$$K_c^{\mathrm{tot}} = \left(\left(\frac{1}{K_c^{\mathrm{in}}}\right)^{2/3} + \left(\frac{1}{K_c^{\mathrm{out}}}\right)^{2/3}\right)^{-3/2}. \tag{5}$$

The inner and outer race contact stiffness coefficients, $K_c{}^{\mathrm{in}}$ and $K_c{}^{\mathrm{out}}$, for the elliptical contact conjunction between two solids can be calculated using the generalized fitted expressions for the elliptic integrals and ellipticity parameter as follows:

$$K_c^{\mathrm{in,out}} = \pi \bar{k}_e E' \sqrt{\frac{R\bar{\xi}}{4.5\bar{\xi}^3}}, \tag{6}$$

where the ellipticity parameter $\bar{k}_e$ and the effective modulus of elasticity $E'$ can be defined as follows [26]:

$$\bar{k}_e = 1.0339\left(\frac{R_y}{R_x}\right)^{0.6360}, \tag{7}$$

$$\frac{1}{E'} = \frac{1}{2}\left(\frac{1-v_a^2}{E_a} + \frac{1-v_b^2}{E_b}\right), \tag{8}$$

where $R_x$ and $R_y$ are the effective radii of the curvature in $x$ and $y$ planes, $v$ is Poisson's ratio of the bearing material and subscripts $a$ and $b$ refer to solids $a$ and $b$, respectively (see Fig. 1). Curvature sum $R$ presented in Eq. (6) can be defined as follows [25]:

$$\frac{1}{R} = \left[\frac{1}{R_x}\right] + \left[\frac{1}{R_y}\right] = \left[\frac{1}{r_{ax}} + \frac{1}{r_{bx}}\right] + \left[\frac{1}{r_{ay}} + \frac{1}{r_{by}}\right], \tag{9}$$

where $r_{ax}$, $r_{ay}$, $r_{bx}$, and $r_{by}$ are radii of the curvature of two solids $a$ and $b$ in two directions, as shown in Fig. 1. It is important to note that in the ball–ring elliptical contact, parameters $r_{bx}$ and $r_{by}$ are negative due to the concave surfaces. Elliptic integrals of the first $\bar{\xi}$ and second $\bar{\zeta}$ kinds presented in Eq. (6) can be expressed as follows:

$$\bar{\xi} = 1.0003 + 0.5968\frac{R_x}{R_y}, \quad \bar{\zeta} = 1.5277 + 0.6023\ \ln\left(\frac{R_y}{R_x}\right). \tag{10}$$

Ball bearing forces can be calculated from the relative radial displacements between the rings, which are denoted as $e_x$ and $e_y$, correspondingly. In Fig. 2, a ball bearing with eccentricities in the $X$- and $Y$-directions is shown. The corresponding radial eccentricity in the direction of ball $i$ can be expressed as follows:

$$e_i^r = e_x \cos\psi_i + e_y \sin\psi_i, \tag{11}$$

where $\psi_i$ is the attitude angle (azimuth angle) of ball $i$.

In Eq. (4), the total elastic deformation can be expressed as follows:

$$\delta_i^{\text{tot}} = 2r + h_0^{\text{in}} + h_0^{\text{out}} - R_{\text{out}} + R_{\text{in}} + e_i^r, \tag{12}$$

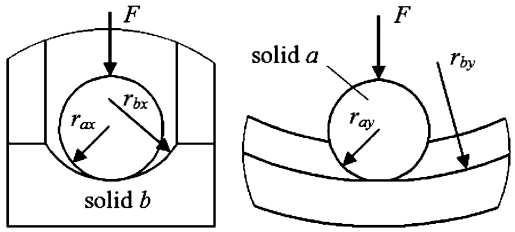


Fig. 1. Ball–ring elliptical contact.

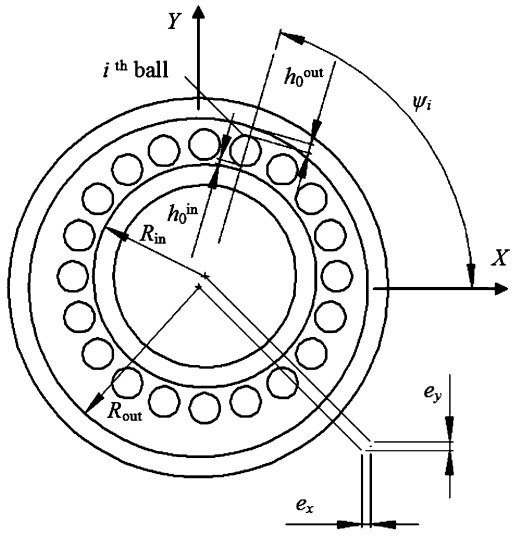


Fig. 2. Axial cross-section of a ball bearing.

where $r$ is the radius of the ball, $h_0^{\text{in}}$ and $h_0^{\text{out}}$ are the lubricant film thicknesses between the contact surfaces and $R_{\text{out}}$ is the outer and $R_{\text{in}}$ is the inner raceway radius. The lubricant film thicknesses are calculated according to the elastohydrodynamic lubrication theory as described in Refs. [16,25].

Finally, the resultant bearing forces acting upon the rotor in radial $X$- and $Y$-directions can be summarized as follows:

$$F_X = -\sum_{i=1}^{z} F_i \cos \psi_i, \quad F_Y = -\sum_{i=1}^{z} F_i \sin \psi_i, \tag{13}$$

where $z$ is the number of balls in the bearing.

### 2.2.2. Bearing friction and inertia

In this section, the bearing friction and the influence of bearing rotational inertia are clarified. The total friction torque of a ball bearing consists of three components and it can be written as follows [27]:

$$T_{\text{fric}} = T_1 + T_2 + T_3, \tag{14}$$

where $T_1$ is the viscous friction torque, $T_2$ is the load-dependent friction torque and $T_3$ is the friction torque caused by rubbing seals. For bearings that operate at relatively low speeds and moderate loads, viscous torque can be expressed as follows [28]:

$$\begin{aligned} T_1 &= 10^{-7} f_0 (\upsilon_0 n_{\text{rev/min}})^{2/3} d_m^3, \quad \upsilon_0 n_{\text{rev/min}} \geqslant 2000 \\ T_1 &= 160 \times 10^{-7} f_0 d_m^3, \quad \upsilon_0 n_{\text{rev/min}} \leqslant 2000, \end{aligned} \tag{15}$$

where $\upsilon_0$ is the kinematic viscosity of the lubricant in centistokes, $n_{\text{rev/min}}$ is the rotation speed given in revolutions per minute, $d_m$ is the pitch diameter of the bearing and $f_0$ is a coefficient that depends on the type of bearing and lubricant. In practice, the values of $f_0$ for deep groove ball bearings range between 0.7 and 2 [28]. Note that this friction torque is independent of the applied load.

The load-dependent friction torque for a deep groove ball bearing with a radial load $F$ can be calculated as follows:

$$T_2 = C_T F d_m \left(\frac{F}{C_0}\right)^{0.55}, \tag{16}$$

where $C_0$ is the static load rating of the bearing and $C_T$ is a variable that varies from 0.0002 to 0.0004. The lower value of the scale pertains to light series bearings while the higher value of the scale pertains to heavy series bearings [28]. In this study, the value of parameter $C_T$ for both retainer bearings is selected to be 0.0003.

If rubbing seals are used in ball bearings, the frictional losses can be greater than those that arise from the bearing itself. In the case of a ball bearing sealed on both sides, the friction torque can be calculated as follows:

$$T_3 = \left(\frac{d_i + D}{20}\right)^2 + 10, \tag{17}$$

where $d_i$ and $D$ are the inner and outer diameter of the bearing, respectively. If only one side of a bearing is sealed, the friction torque must be divided by 2 [29]. It must be noted that these empirical equations are unit sensitive; friction torque is expressed in N mm, loads and forces are expressed in N, dimensions are expressed in mm and viscosity in cSt ($\text{mm}^2/\text{s}$).

In this study, the rotational inertias of the balls as well as the inertia of the inner ring are accounted for in the ball bearing model. The combined inertia of the ball bearing can be derived with the help of the total kinetic energy of the ball bearing, $E_{bb,c}$, as follows:

$$E_{bb,c} = E_{\text{ir},r} + zE_{b,r} + zE_{b,k} = \frac{1}{2} J_{bb,c} \omega_{\text{ir}}^2, \tag{18}$$

where $E_{\text{ir},r}$ is the rotational kinetic energy of the inner ring, $E_{b,r}$ is the kinetic energy due to the rotation of a ball around its own axis and $E_{b,k}$ is the kinetic energy of a ball due to its circumferential movement. In Eq. (18), $J_{bb,c}$ is the combined inertia of the bearing and $\omega_{\text{ir}}$ is the angular velocity of the inner ring. Neglecting

the combined inertia of the ball bearing can lead to an inaccurate model. The inertia of the inner ring and balls is particularly important when the inertia of the inner ring is small compared to the combined inertia of the bearing. For example, for the ball bearings used in this study (see Table 2) the effect of the combined inertia is more than 21% compared to a case where only the inertia of the inner ring of the bearing is accounted for.

### 2.3. Model of the contact

The contact model of the rotor and the retainer bearings includes descriptions of contact forces and friction. Contact between the rotor and the bearing can be modeled using a nonlinear circle-in-circle contact as depicted in Fig. 3. This type of contact model has been studied extensively and can be found, for example, in Refs. [30,31]. The radial contact force $F_r$ is a function of the contact penetration and the penetration velocity. The radial contact force, which affects the rotor, can be written as follows:

$$F_r = \begin{cases} K\delta^{3/2}\left(1+\frac{3}{2}C\dot{\delta}\right), & e_r \geqslant c_r \text{ and } F_r > 0, \\ 0, & e_r < c_r \text{ or } F_r \leqslant 0, \end{cases} \tag{19}$$

where $K$ is the stiffness and $C$ is the damping of the contact. In Eq. (19), $e_r$ represents the radial displacement of the rotor, $c_r$ is the radial clearance between the rotor and the inner ring of the retainer bearing, i.e., an air gap, $\delta$ is the depth of penetration of the contact and $\dot{\delta}$ is its derivative with respect to time. In Eq. (19), negative contact forces are avoided by ignoring contact whenever the contact force becomes negative [32]. The $X$- and $Y$-components of the radial contact force $F_r$ can be calculated using the geometry presented in Fig. 3. Eq. (19) is based on the Hertzian contact theory for two spheres and it assumes that the impact velocity is below 500 mm/s [33]. The classical contact theory presented above is used widely in drop-down simulations. Fumagalli and Schweitzer [34] as well as von Groll and Ewins [35,36] used similar models of contact in their research. The penetration $\delta$ between the rotor and the inner ring of the bearing can be expressed as follows:

$$\delta = e_r - c_r. \tag{20}$$

As shown in Fig. 3, the radial displacement between the rotor and the inner ring of the bearing with respect to the center of the bearing can be obtained from the displacements along the $X$- and $Y$-axis as follows:

$$e_r = \sqrt{e_{x,r}^2 + e_{y,r}^2}. \tag{21}$$

Radial clearance in the contact can be obtained using the radii of the rotor $r_r$ and the inner ring $r_i$ as follows:

$$c_r = r_i - r_r. \tag{22}$$

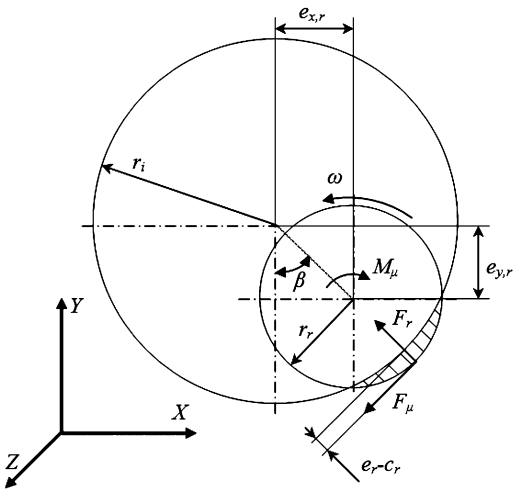


Fig. 3. Circle-in-circle contact.

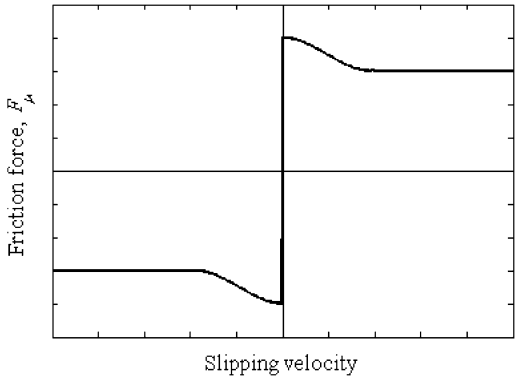


Fig. 4. Friction force between the rotor and the inner ring of the bearing in the combined friction model.

The magnitude of the friction force which acts at the center of the rotor and is perpendicular to the radial contact force can be calculated as follows:

$$F_\mu = \mu F_r, \tag{23}$$

where $\mu$ is the coefficient of friction between the rotor and the inner ring of the bearing. The friction coefficient can be defined as a function of the slipping velocity between the rotor and the inner ring of the bearing. In this study, the coefficient is defined using two different models. The first friction model is defined employing Coulomb friction with a constant friction coefficient. The second friction model is a combination of the Coulomb, Stribeck and static friction models. The model determines the maximum static friction coefficient as well as the sliding friction coefficient [37,38]. An example of the friction force calculated by using the combined friction model is presented in Fig. 4. Because the friction force is assumed to act in the center of the rotor it causes a torque in the direction opposite to the direction of rotation. This torque can be expressed as follows:

$$M_\mu = F_\mu r_r. \tag{24}$$

### 2.4. Aerodynamic torque

In the case of power failure, the rotor decelerates due to the friction torque of the retainer bearings. In many applications, the aerodynamic torque has a vital role in the deceleration of the rotor. Schmied and Pradetto [39] have introduced a model for the aerodynamic torque to describe the deceleration of the rotor as follows:

$$n = \frac{n_0}{1 + at}, \tag{25}$$

where $n$ is the speed of the rotor at time $t$ from the failure, $n_0$ is the speed at the instant of the failure and $a$ is a deceleration factor. The deceleration factor depends on the load as well as the geometry of the rotor. The deceleration factor can be defined experimentally. In this research, the deceleration factor is assumed to be $0.1\,\mathrm{s}^{-1}$ [39].

The aerodynamic torque which affects the rotor can be calculated as follows:

$$M_{\mathrm{ad}} = I_p \dot{n}, \tag{26}$$

where $\dot{n}$ is a derivative of $n$ with respect to time.

## 3. Numerical results

In this section, a simulation approach introduced in the previous section is used to study responses of a rotor during a drop-down. The structure under investigation is an electrical motor, whose rotor is supported by two AMBs. The studied rotor is shown in Fig. 5. Both AMBs ($AMB_1$ and $AMB_2$ in Fig. 5) generate independent support forces $F_{\mathrm{AMB1}}$ and $F_{\mathrm{AMB2}}$. Both support forces are assumed to close down immediately when a fault situation occurs. Accordingly, it is assumed in this study that the collapsing magnetic force has

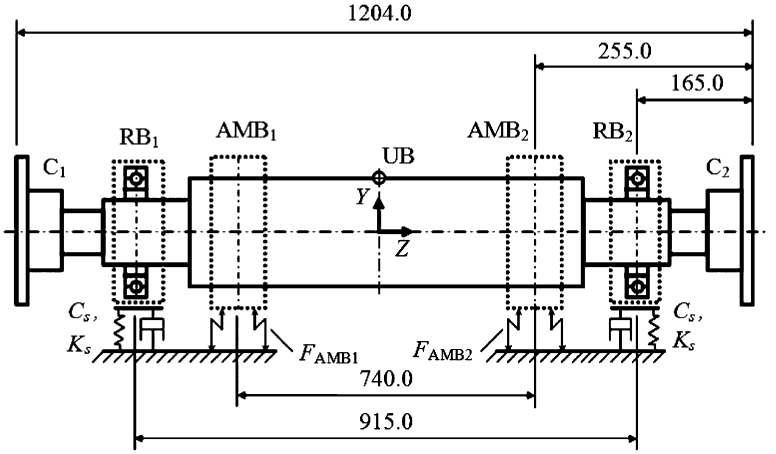


Fig. 5. Diagram of the electric motor under investigation (dimensions are in millimeters).

Table 1
Parameters of the studied electric motor and the contact

| Dimension and property | Specification |
|---|---|
| Mass of rotor system, $m_r$ | 54.1 kg |
| Polar moment of inertia of rotor, $I_{p,r}$ | 0.07 kg m$^2$ |
| Diametral moment of inertia of rotor, $I_{d,r}$ | 7.41 kg m$^2$ |
| Mass of couplings, $m_c$ | 5.6 kg |
| Polar moment of inertia of couplings, $I_{p,c}$ | 0.015 kg m$^2$ |
| Diametral moment of inertia of couplings, $I_{d,c}$ | 0.010 kg m$^2$ |
| Air gap between rotor and bearings, $c_r$ | 300 μm |
| Stiffness coefficient of contact, $K$ | $5 \times 10^8$ N/m |
| Damping coefficient of contact, $C$ | 1000 N s/m |

no effect on the dynamic behavior of the rotor during the drop-down. The structure includes retainer bearings which have a vital role in an emergency drop-down. The air gaps between the inner rings of the retainer bearings and the rotor are half of the air gaps of the AMBs. The outer rings of the retainer bearings are assumed to be rigidly attached to the bearing housings. In the simulation model, the bearing housings have only two degrees of freedom that are translations in the global $X$- and $Y$-directions. The bearing housings are connected to the ground with linear spring-dampers in the $X$- and $Y$-directions. The dimensions of the entire rotor system are shown in Table 1 while the parameters of the retainer bearings used are shown in Table 2. The direction of gravity is the negative $Y$-direction. The unbalance mass UB is located in the middle of the rotor at an angle of 90° from the positive $X$-axis. The masses and moments of inertia of the couplings ($C_1$ and $C_2$ in Fig. 5) at both ends of the rotor are given in Table 1. In addition, the parameters for the contact model between the rotor and the retainer bearings are shown in Table 1.

The rotor is made of steel, and its density $\rho$ is assumed to be 7800 kg/m$^3$. The inertia of AMB laminations is accounted for in the rotor model while the shear and the elastic modulus of laminations are assumed to be zero. Due to the displacement sensors of the control system of the AMBs, aluminum sleeves are assembled on the rotor. The translational displacements and forces are predicted from both retainer bearings. The numerical integrator used in this study is the fourth order Runge–Kutta [40] method with a time step of $1.5 \times 10^{-5}$ s.

### 3.1. Modal analysis

In order to validate the simulation model, an experimental modal analysis is carried out on the rotor system. In the experiment, the rotor is hoisted using flexible rubber ropes. As a consequence, the effects of the support

Table 2
Parameters of the retainer bearings

| Dimension and property | Specification | | |
|---|---|---|---|
| Number of bearing | $RB_1$ | | $RB_2$ |
| Type of bearing | | Deep-groove ball bearing | |
| Inner diameter, $d_i$ (mm) | 75.0 | | 70.0 |
| Outer diameter, $D$ (mm) | 95.0 | | 90.0 |
| Bearing width, $B$ (mm) | 10.0 | | 10.0 |
| Pitch diameter, $d_m$ (mm) | 85.0 | | 80.0 |
| Ball radius, $r$ (mm) | 2.8 | | 2.8 |
| Static load rating, $C_0$ (N) | 14 300 | | 13 200 |
| Number of balls, $z$ | 27 | | 25 |
| Diametral clearance, $c_{d,b}$ (μm) | | 15 | |
| Bearing damping coefficient, $C_b$ (N s/m) | | 250 | |
| Inner and outer race conformity, $R_r$ | | 0.52 | |
| Modulus of elasticity, $E$ (MPa) | | 207 000 | |
| Poisson's ratio, $v$ | | 0.3 | |
| Viscosity of lubricant, $v_0$ (cSt) | | 25.0 | |

Table 3
Measured and calculated free–free frequencies of the studied rotor

| Mode # | Measured frequency (Hz) | Calculated frequency (Hz) | Difference (%) | Measured damping (%) |
|---|---|---|---|---|
| 1 | 193.5 | 193.5 | 0.0 | 0.164 |
| 2 | 397.0 | 414.0 | +1.5 | 0.055 |
| 3 | 767.5 | 790.7 | +0.8 | 0.064 |
| 4 | 1238.0 | 1341.1 | +2.7 | 0.116 |

on the natural frequencies and modes of the rotor are minimized. The measurement is carried out by employing a roving hammer procedure, where the accelerometer position is fixed and the hammering points are varied along the rotor. The hammering impulses are applied horizontally in order to minimize the effect of the rubber ropes on rotor damping. The modal analysis is performed for the rotor with stacks of steel laminations and couplings. Measured and calculated natural frequencies as well as measured damping ratios are presented in Table 3.

It can be concluded from the results that the calculated natural frequencies are slightly higher than the measured ones. This is typical for beam models where the cross-section deformation of the element is ignored. In addition, the beam finite element used in this study does not account for discontinuities in the shear force. This may be one reason for the discrepancy between the calculated and measured frequency [41]. It is noteworthy that the studied rotor includes structural irregularities. One irregularity is friction between jointed components. The friction is particularly difficult to define because the sleeves and the laminations are not fitted on the rotor. The most significant irregularity is the stacks of steel laminations. Because of the structure of the laminations, they are modeled without any bending stiffness. In practice, the laminations may carry some bending load.

### 3.2. Simulation results

The dynamic behavior of the rotor system during the drop on retainer bearings is studied using a detailed simulation model introduced in previous section. In the first example, the effect of the number of selected free-free modes of the rotor on the behavior of the rotor system during drop-down is studied. The second example presents simulation results of the drop-down and the deceleration of the rotor under the natural frequency of the first free-free mode of the rotor. The effect of friction coefficients in the contact between the rotor and the

retainer bearing is studied in the third example. Coulomb and combined friction models are also compared in this example. In the fourth example, the effect of the radial clearance of the retainer bearings on the behavior of the rotor is examined. In the numerical examples, the unbalance mass $m_{ub}$ is assumed to be 1 g with an eccentricity of 42.5 mm, the stiffness of the support $K_s$ is assumed to be $3 \times 10^8$ N/m and the damping of the support $C_s$ is assumed to be 5000 N s/m. The total time of the simulation is 0.1 s and the initial angular velocity of the steady-state rotor is assumed to be 15 000 rev/min. In this study, it is assumed that the rotor experiences no vibration before contact with the retainer bearings. In other words, it is assumed that the unbalance compensation of the AMBs is functioning properly before drop-down. In this section, all the presented results are monitored from the node in the location of retainer bearing 2 ($RB_2$ in Fig. 5).

### 3.2.1. Number of flexible modes

The effect of the number of selected flexible modes of the rotor on orbit prediction is examined in this section. Five sets of modes are used in the numerical examples. The number of modes in the sets varies from 8 to 32 with steps of eight. In addition, one set includes only four selected modes. Solutions obtained using five sets of modes are compared against the reference solution in which 56 modes are used. The orbits of the rotor with different numbers of selected flexible modes of the rotor are shown in Fig. 6. It can be seen from the figure that, one hand, by using eight free-free modes, the results are significantly more accurate than by using four modes. On the other hand, the use of 32 modes yields nearly as accurate a result as by using 56 modes. Thus it can be concluded that the use of eight selected modes in this example leads to an acceptable solution while the use of 32 selected modes leads to a practically identical solution as the use of 56 selected modes. It is noteworthy that the response of a mode needs to be described with a corresponding differential equation. For this reason, the reduction of the modes has a direct influence on the number of the differential equations and, consequently, on the CPU time consumption.

The reason for the inaccurate description when using four elastic modes is the impacts between the rotor and retainer bearings during the drop-down. The impacts excite eigenmodes which have even higher frequencies than the fourth bending mode of the rotor can describe.

### 3.2.2. Unstabilizing effect of natural frequency

Deceleration above the speed of the first free–free frequency during the drop-down of the rotor is studied in this section. The initial angular velocity of the rotor at the instant of the drop-down is selected to be

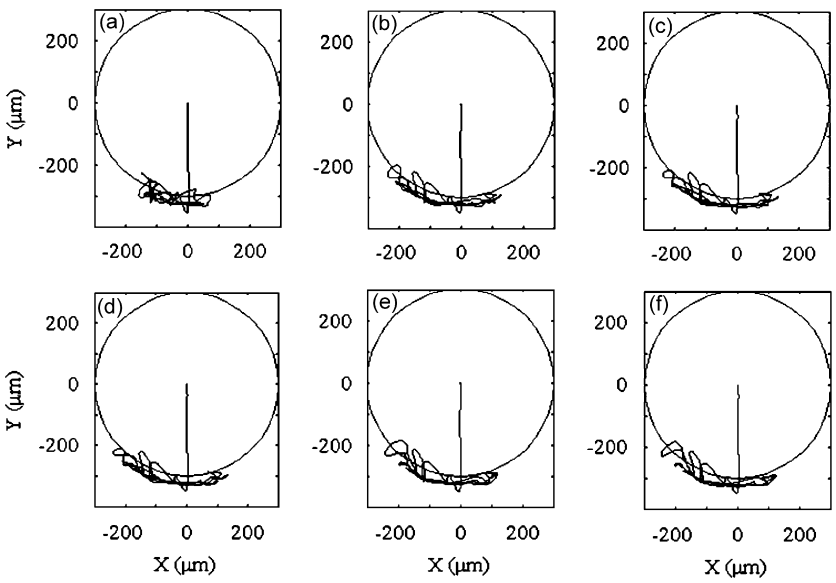


Fig. 6. Orbit of the rotor by using: (a) 4, (b) 8, (c) 16, (d) 24, (e) 32 and (f) 56 selected flexible modes. The circle indicates the air gap of the retainer bearing and the line the orbit of the rotor.

12 500 rev/min while the aerodynamic torque is assumed to be four times smaller than in other simulations. Thus the contribution of the first free–free frequency of the rotor to the dynamic response is emphasized. The rotor system under investigation is slightly modified after the experimental modal analysis. In the modification, one additional sleeve is added to the rotor. This increased the first calculated free–free frequency of the rotor to 197.0 Hz.

Fig. 7 shows the vertical displacements of the rotor during the deceleration. It can be seen in the figure that vibration increases when the rotational velocity of the rotor decelerates under 11 700 rev/min (195.0 Hz). This is due to the excitation of the first free–free mode of the rotor. The greatest response occurs about 2 Hz below the first free–free frequency. This is consistent with the general vibration theory of decelerating rotors [42]. A part of the discrepancy may be due to the fact that the rotor system is not unsupported all of the time. The contact of the rotor with the bearings introduces a support that results in decreasing the lowest natural frequency of the rotor system. For this reason, the reference condition of the eigenvalue analysis should be selected with care [43].

The spectrum of the vertical velocity of the rotor is presented in Fig. 8. It can be seen from the figure that the first free-free mode, 197.0 Hz, contributes to a peak in the acceleration rate of the rotor. The increased acceleration rate, in turn, influences the contact and support forces. Peaks in lower frequencies, 55 and 60 Hz,

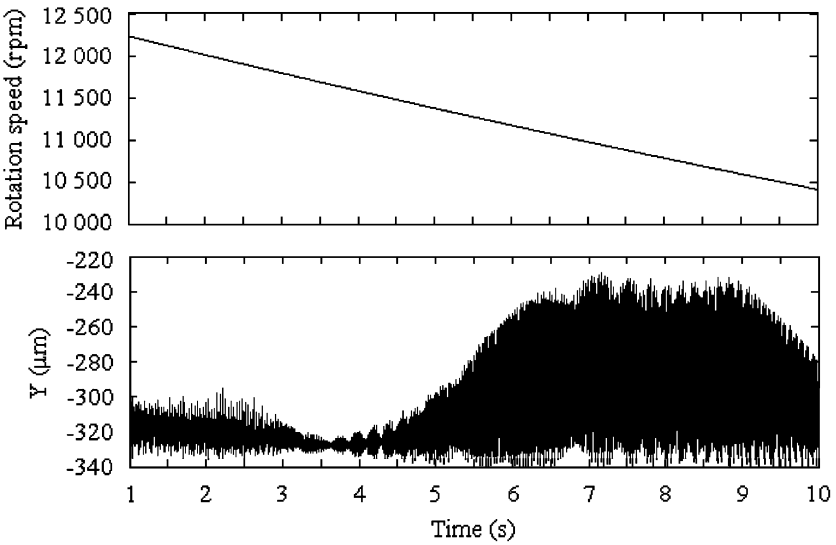


Fig. 7. Response of the rotor in vertical direction.

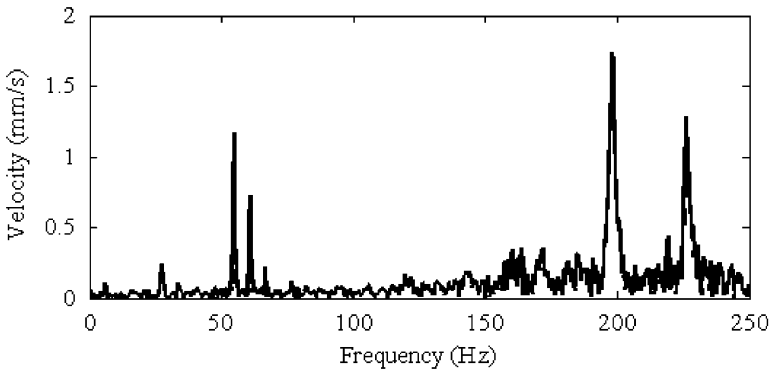


Fig. 8. The spectrum of the vertical velocity of the rotor from 0 to 250 Hz.

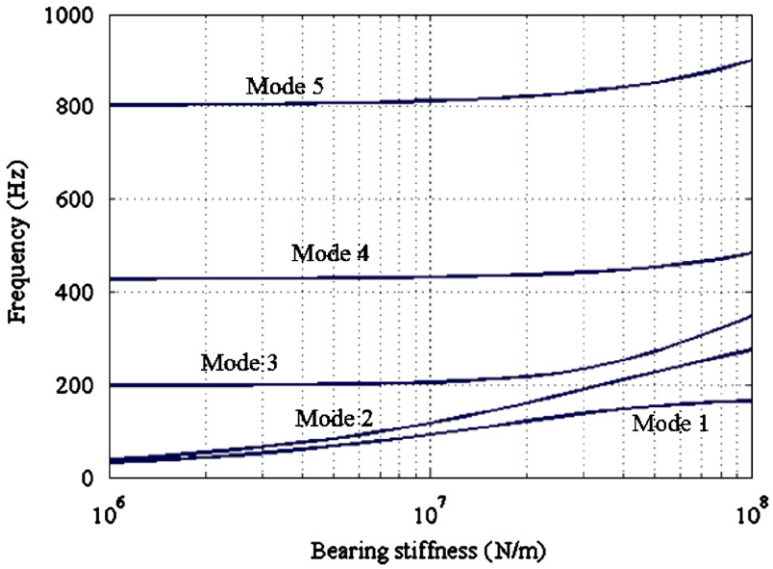


Fig. 9. Critical speed map of the supported rotor.

are caused by the eigenfrequencies of the supported rotor. The second and third natural frequency can be seen clearly in Fig. 9, where the critical speed map of the rotor is depicted. As can be seen from the critical speed map, the first frequency is higher than 197.0 Hz. The reason for this is the fluctuations in the rotor supporting conditions, as explained above. This kind of fluctuation is difficult to take into account in practice because it is occasional and depends on many parameters and the structure itself [44].

*3.2.3. Effects of friction coefficient and models*

In this section, the behavior of the rotor during its drop-down is studied using different friction coefficients together with two different friction models. The first model is a simple Coulomb friction model, whereas the second one is a combined friction model which is based on the Coulomb, Stribeck and static friction models. In the combined friction model, the static friction coefficient is in all of the cases 0.05 higher than the dynamic friction coefficient.

Fig. 10 shows the orbits of the rotor when the Coulomb friction model is used. It can be seen from the results that the rotor does not undergo a whirling motion when the friction coefficient between the rotor and the retainer bearings is below 0.45. This can also be seen from Fig. 11, which presents the orbits when the combined friction model with different friction coefficients is used. Figs. 10 and 11 show that the orbit of the rotor becomes larger when the friction coefficient increases. This can be observed even before the rotor starts to whirl. In the whirling motion, the displacements of the rotor increase significantly. It can be concluded from the results that the largest displacement of the rotor does not take place immediately after the drop-down, as in the case of the lower friction coefficients. Instead, the greatest response occurs after 0.08 s of the drop-down. After this instant, the response, i.e., the orbit of the rotor, are stabilized. The orbit of the rotor does not stay inside the static retainer bearing (the circle in Figs. 10 and 11) after the drop-down. The reason for this is that the retainer bearings are assembled elastically on the ground and the bearing model is able to describe the elasticity of the bearing.

The effects of the friction coefficient between the rotor and retainer bearings on the dynamic responses are examined widely. However, it is important to note that the friction coefficient alone does not determine the behavior of the rotor during the drop-down. Many other parameters, such as stiffness and damping properties of the support, mass of the support device, balancing of the rotor and, naturally, the structure of the rotor system determine the behavior of the structure. Ecker [8] examined the effects of friction to the rotor responses and noticed that high friction coefficients can lead to a backward whirling motion of the rotor. This is an important observation because in magnetic bearing applications a contaminant free environment is often

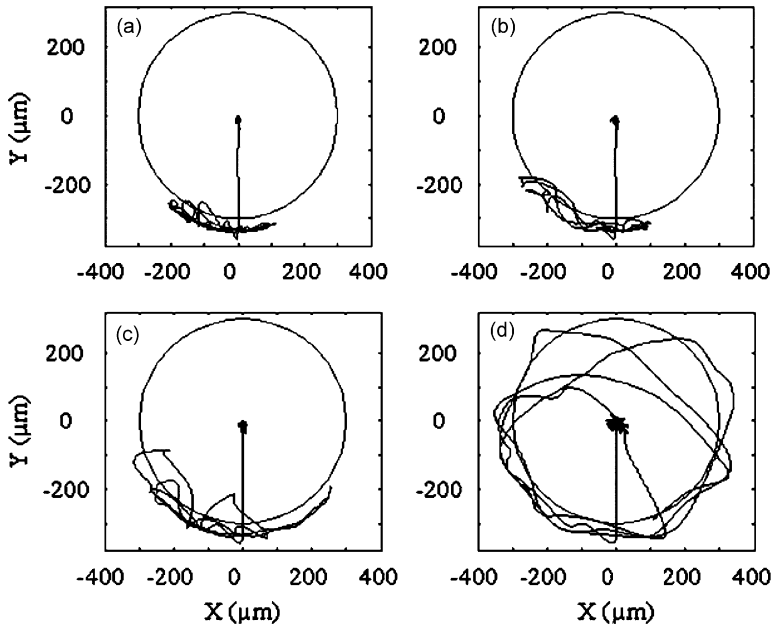


Fig. 10. Orbit of the rotor by using the Coulomb friction model. The friction coefficient varies: (a) 0.15, (b) 0.25, (c) 0.35 and (d) 0.45. The line in the middle of the circle describes the displacement of the support.

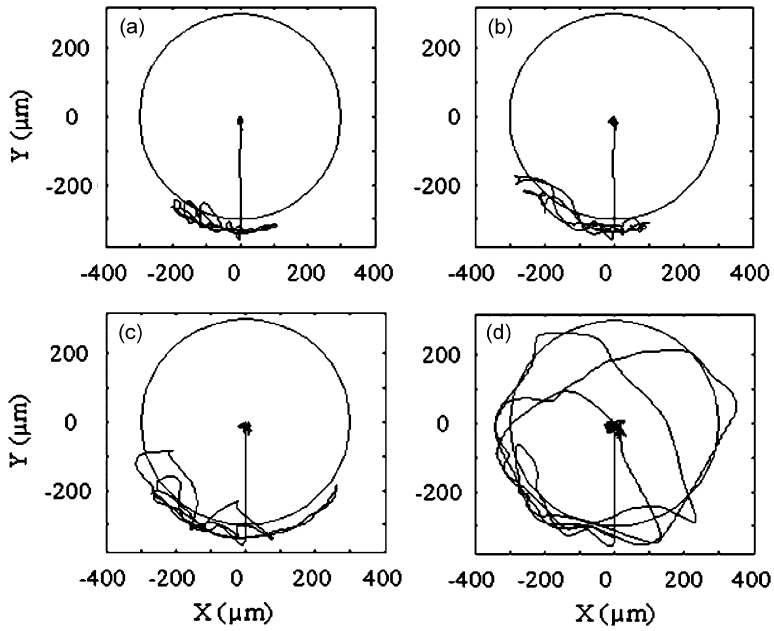


Fig. 11. Orbit of the rotor by using a combined friction model. The friction coefficient varies: (a) 0.15, (b) 0.25, (c) 0.35 and (d) 0.45. The line in the middle of the circle describes the displacement of the support.

required. This means, in turn, that the retainer bearings are required to be dry and thus without lubrication. Furthermore, Fumagalli and Schweitzer [45] noted that a low coefficient of friction is a beneficial feature for the retainer bearings. It is important to note that the coefficient of friction may not be constant. This is due to wearing that can occur during the interaction between the rotor and retainer bearings and, thereby, increase

the friction. Sun [46] examined the thermal growth of the retainer bearings during the contact. He noted that the rotor drop dynamics and thermal growth drastically change when the friction coefficient increases. Because of a larger friction force, the orbit of the rotor expands after drop-down and the direction of the first bounce approaches the tangential direction of the contact point. Hence, it is important to find a threshold friction coefficient above which the rotor enters into a high-speed backward whirl. Therefore, reducing the friction coefficient plays a critical role in the stability of the rotor drop dynamics. A fine surface finish and powder or solid lubricants can be utilized on the contact area, if it is acceptable in practice. In this study, the AMB system needs a high friction coefficient between the rotor and bearings in order to cause a full backward whirling motion of the rotor. This is in agreement with previous examination of retainer bearings [44]. From a practical point of view, simulated predictions of the orbit may carry some uncertainties. The main source of uncertainty is a constant friction coefficient which does not account for the increase of the friction coefficient resulting from thermal expansion and wearing in inner rings [14].

From Figs. 10 and 11 it can be concluded that different friction models lead to practically identical results. It is noteworthy that the effect of the static friction coefficient is insignificant even when the rotor is stabilizing from the whirling motion. For this reason, it can be noted that a Coulomb friction model leads to acceptable results during the rotor drop on retainer bearings. It is worth mentioning that the combined friction model is computationally more expensive than the Coulomb friction.

### 3.2.4. *Effect of retainer bearing's radial clearance*

In the last numerical example, the effect of the radial clearance of the retainer bearings on the behavior of the rotor is examined. The clearances are varied from zero clearance to C3 via the normal and C2 clearance. The magnitude and direction of the contact force with the above presented clearances of the retainer bearings are shown in Fig. 12. The effect of radial clearance is minor but observable. Based on the numerical results, enlarged clearance results in a more indefinite orbit. This means that the magnitude of the contact forces increased, as can be seen in the figure. It is also important to note that due to the geometry of the large

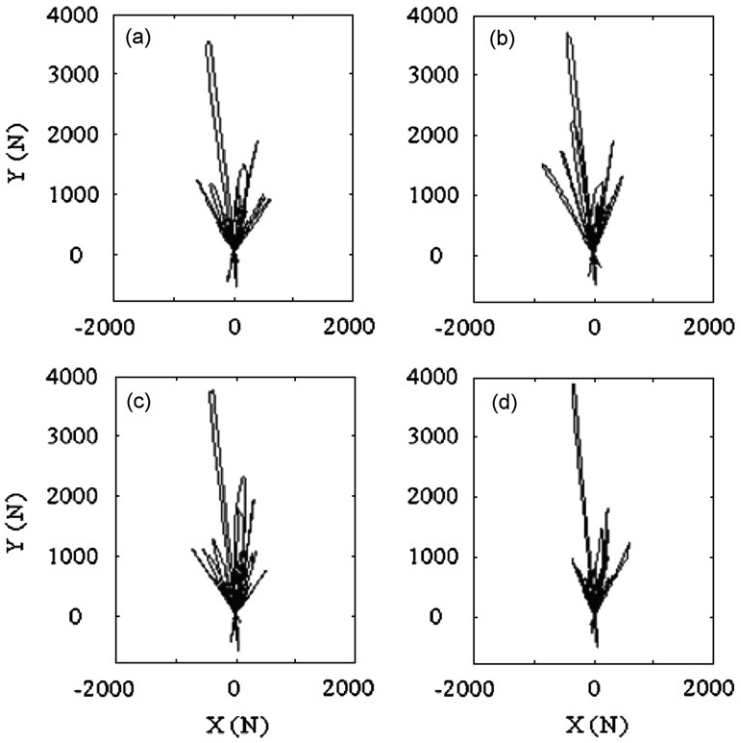


Fig. 12. Magnitude and direction of the contact force with different clearances ((a) zero clearance, (b) C2 clearance, (c) normal clearance, (d) C3 clearance) of the retainer bearing.

clearance bearing, the individual ball is imposed by larger loading than a ball in the same position in the case of a small clearance bearing or preloaded bearing. This is due to the fact that in a preloaded bearing, the loading is distributed more evenly between several balls. Thus it is recommendable to use preloaded bearings instead of a bearing with a large clearance if the thermal expansion does not cause severe problems.

## 4. Conclusions

In this study, the dynamics of an AMB supported rotor during the drop-down on retainer bearings was studied employing a detailed simulation model. The studied structure included a rotor, two AMBs and two retainer bearings. The retainer bearings were described using a detailed ball bearing model, which accounts for damping and stiffness properties, oil film, inertia of rolling elements and friction between races and rolling elements. The rotor was modeled as a flexible body by using the beam finite elements based on the Timoshenko theory.

In this study, the simulation response of the rotor during the drop-down was analyzed using a component mode synthesis. This approach is numerically efficient and may be utilized in a real-time control application. Using the developed model, the effects of the number of selected flexible modes on the prediction of the orbits of the rotor were discussed. The effects of free–free natural frequencies of the rotor during rotor deceleration on the orbit of the rotor were also studied. It was noticed in the examination that the responses of the rotor grew when the rotational velocity of the rotor went under the first natural frequency. The same behavior was noticed from the spectrum of the vertical velocity and the critical speed map. Furthermore, the effect of different friction models as well as the effect of the radial clearance of retainer bearings on the behavior of rotor was examined. From the simulated scenarios it can be concluded that the effect of the friction models on the orbit of the rotor was not significant. The effects of the friction coefficient were in good agreement with the other studies available in the literature. The study of the radial clearance of the retainer bearings revealed that the effect of the clearance on the dynamic behavior of the rotor is insignificant.

## References

[1] G. Schweitzer, H. Bleuler, A. Traxler, *Active Magnetic Bearings—Basics, Properties and Applications*, vdf Hochschulverlag AG, Zurich, 1994.

[2] T. Ishii, R.G. Kirk, Transient response technique applied to active magnetic bearing machinery during rotor drop, *ASME Journal of Vibration and Acoustics* 118 (1996) 154–163.

[3] M. Orth, R. Erb, R. Nordmann, Investigations of the behavior of a magnetically suspended rotor during contact with retainer bearings, *Proceedings of the Seventh International Symposium on Magnetic Bearings*, Zurich, Switzerland, 2000, pp. 33–38.

[4] M.A. Fumagalli, Modelling and Measurement Analysis of the Contact Interaction between a High Speed Rotor and its Stator, PhD Thesis, Swiss Institute of Technology, 1997.

[5] P. McMullen, V. Vuong, L. Hawkins, Flywheel energy storage system with AMB's and hybrid backup bearings, *Proceedings of the 10th International Symposium on Magnetic Bearings*, Martigny, Switzerland, 2006.

[6] H.M. Chen, J. Walton, H. Heshmat, Zero clearance auxiliary bearings for magnetic bearing systems, *Proceedings of the 42nd International Gas Turbine and Aeroengine Congress and Exposition*, Orlando, USA, 1997.

[7] H. Ulbrich, A. Chavez, L. Ginzinger, Control of impact phenomena of a rubbing rotor, *Proceedings of the Third International Symposium on Stability Control of Rotating Machinery*, Cleveland, USA, 2005.

[8] H. Ecker, Nonlinear stability analysis of a single mass rotor contacting a rigid backup Bearing, *Proceedings of the Euromech Colloquium*, Loughborough, UK, 1998, pp. 79–89.

[9] S. Zeng, Motion of AMB rotor in backup bearings, *ASME Journal of Vibration and Acoustics* 124 (2002) 460–464.

[10] M.O.T. Cole, P.S. Keogh, C.R. Burrows, The dynamic behavior of a rolling element auxiliary bearing following rotor impact, *ASME Journal of Tribology* 124 (2002) 406–413.

[11] M.O.T. Cole, P.S. Keogh, C.R. Burrows, Predictions on the dynamic behaviour of a rolling element auxiliary bearing for rotor/AMB systems, *Proceedings of the Eighth International Symposium on Magnetic Bearings*, Mito, Japan, 2002, pp. 501–506.

[12] K.V.S. Raju, K. Ramesh, E.E. Swanson, R.G. Kirk, Simulation of AMB turbomachinery for transient loading conditions, *Proceedings of the MAG'95 Magnetic Bearings, Magnetic Drives, and Dry Gas Seals Conference & Exhibition*, Alexandria, USA, 1995, pp. 227–235.

[13] E.E. Swanson, R.G. Kirk, J. Wang, AMB rotor drop initial transient on ball and solid bearings, *Proceedings of the MAG'95 Magnetic Bearings, Magnetic Drives, and Dry Gas Seals Conference & Exhibition*, Alexandria, USA, 1995, pp. 207–216.

[14] S. Zeng, Modelling and experimental study of the transient response of an active magnetic bearing rotor during rotor drop on back-up bearings, *Proceedings of the Institution of Mechanical Engineers. Part I. Journal of Systems & Control Engineering* 217 (2003) 505–517.
[15] E.N. Cuesta, N.I. Montbrun, V. Rastelli, S.E. Diaz, Simple model for a magnetic bearing system operating on the auxiliary bearing, *Proceedings of the GT2005 ASME Turbo Expo 2005*, Reno-Tahoe, USA, 2005, pp. 891–898.
[16] J. Sopanen, A. Mikkola, Dynamic model of a deep groove ball bearing including localized and distributed defects, Part 1: theory, *Proceedings of the Institution of Mechanical Engineers, Journal of Multi-Body Dynamics* 217 (K) (2003) 201–211.
[17] J. Sopanen, A. Mikkola, Dynamic model of a deep groove ball bearing including localized and distributed defects, Part 2: implementation and results, *Proceedings of the Institution of Mechanical Engineers, Journal of Multi-Body Dynamics* 217 (K) (2003) 213–223.
[18] H.D. Nelson, J.M. McVaugh, The dynamics of rotor bearing systems using finite elements, *Journal of Engineering for Industry* 98 (1976) 593–600.
[19] W.J. Chen, E.J. Gunter, *Introduction to Dynamics of Rotor-Bearing Systems*, Trafford Publishing, Victoria, 2005.
[20] K.J. Bathe, *Finite Element Procedures*, Prentice-Hall, Englewood Cliffs, NJ, 1996.
[21] D.J. Ewins, *Modal Testing: Theory, Practice and Application*, second ed., Research Studies Press Ltd., Somerset, 2000.
[22] G. Genta, *Vibration of Structures and Machines*, third ed., Springer, New York, 1998.
[23] M. Orth, R. Nordmann, Aneas, a modeling tool for nonlinear analysis of active magnetic bearing systems, *Proceedings of the IFAC Conference of Mechatronic Systems*, Berkeley, USA, 2002.
[24] M. Helfert, M. Ernst, R. Nordmann, B. Aeschlimann, High-speed video analysis of rotor-retainer-bearing-contacts due to failure of active magnetic bearings, *Proceedings of the 10th International Symposium on Magnetic Bearings*, Martigny, Switzerland, 2006.
[25] B.J. Hamrock, *Fundamentals of Fluid Film Lubrication*, McGraw-Hill, New York, 1994.
[26] D.E. Brewe, B.J. Hamrock, Simplified solution for elliptical-contact deformation between two elastic solids, *Journal of Lubrication Technology* 99 (1977) 485–487.
[27] W. Changsen, *Analysis of Rolling Element Bearings*, Mechanical Engineering Publications Ltd., London, 1991.
[28] T.A. Harris, *Rolling Bearing Analysis*, third ed., Wiley, New York, 1990.
[29] SKF, SKF Bearing Handbook, Turin, 1991.
[30] A. Bartha, Dry friction induced backward whirl: theory and experiment, *Proceedings of the Fifth International IFToMM Conference on Rotor Dynamics*, Darmstadt, Germany, 1998, pp. 768–779.
[31] A. Bartha, Dry Friction Backward Whirl of Rotors, PhD Thesis, Swiss Institute of Technology, 2000.
[32] R. Markert, G. Wegener, Transient vibration of elastic rotors in retainer bearings, *Proceedings of the Seventh International Symposium on Transport Phenomena and Dynamics of Rotating Machinery*, Honolulu, USA, 1998, pp. 764–774.
[33] K.H. Hunt, F.R. Crossley, Coefficient of restitution interpreted as damping in vibroimpact, *ASME Journal of Applied Mechanics* 42 (1975) 440–445.
[34] M. Fumagalli, G. Schweitzer, Measurements on a rotor contacting its housing, *Proceedings of the Sixth International Conference on Vibrations in Rotating Machinery*, Oxford, United Kingdom, 1996, pp. 779–788.
[35] G. von Groll, D.J. Ewins, A mechanism of low subharmonic response in rotor/stator contact-measurements and simulations, *Journal of Vibration and Acoustics* 124 (2002) 350–358.
[36] G. von Groll, Windmilling in Aero-Engines, PhD Thesis, University of London, 2000.
[37] H. Olsson, K.J. Aström, C. Canudas de Wit, M. Gäfvert, P. Lischinsky, Friction models and friction compensation, *European Journal of Control* 4 (1998) 176–195.
[38] J.L. Ha, R.F. Fung, C.F. Han, J.R. Chang, Effects of frictional models on the dynamic response of the impact drive mechanism, *Journal of Vibration and Acoustics* 128 (2006) 88–96.
[39] J. Schmied, J.C. Pradetto, Behaviour of a one ton rotor being dropped into auxiliary bearings, *Proceedings of the Third International Symposium on Magnetic Bearings*, Alexandria, USA, 1992, pp. 145–156.
[40] E. Hairer, S.P. Norsett, G. Wanner, *Solving Ordinary Differential Equations I: Nonstiff Problems*, Springer, New York, 1993.
[41] E. Lantto, Finite Element Model for Elastic Rotating Shaft, Licentiate Thesis, Helsinki University of Technology, 1997.
[42] T. Yamamoto, Y. Ishida, *Linear and Nonlinear Rotordynamics: A Modern Treatment with Applications*, Wiley, New York, 2001.
[43] A.A. Shabana, *Dynamics of Multibody Systems*, second ed., Wiley, New York, 1998.
[44] W.C. Foiles, P.E. Allaire, Nonlinear transient modeling of active magnetic bearing rotors during rotor drop on auxiliary bearing, *Proceedings of the MAG'97 Industrial Conference and Exhibition on Magnetic Bearings*, Alexandria, USA, 1997, pp. 154–163.
[45] M. Fumagalli, G. Schweitzer, Motion of rotor in rigid retainer bearings, *Proceedings of the Fifth International Symposium on Magnetic Bearings*, Kanazawa, Japan, 1996, pp. 509–514.
[46] G. Sun, Rotor drop and following thermal growth simulation using detailed auxiliary bearing and damper models, *Journal of Sound and Vibration* 289 (2006) 334–359.